Soft Matter

PAPER

View Article Online
View Journal | View Issue

Cite this: *Soft Matter*, 2014, **10**, 5061

Generalized phase behavior of cluster formation in colloidal dispersions with competing interactions†

P. Douglas Godfrin,[a] Néstor E. Valadez-Pérez,[b] Ramon Castañeda-Priego,[b] Norman J. Wagner*[a] and Yun Liu*[ac]

Received 30th December 2013
Accepted 1st May 2014

DOI: 10.1039/c3sm53220h

www.rsc.org/softmatter

Colloidal liquids interacting with short range attraction and long range repulsion, such as proposed for some protein solutions, have been found to exhibit novel states consisting of equilibrium particle clusters. Monte Carlo simulations are performed for two physically meaningful inter-particle potentials across a broad range of interaction parameters, temperatures and volume fractions to locate the conditions where clustered states are found. A corresponding states phase behavior is identified when normalized by the critical point of an appropriately selected reference attractive fluid. Clustered fluid states and cluster percolated states are found exclusively within the two phase region of the state diagram for a reference attractive fluid, confirming the underlying intrinsic relation between clustered states and bulk phase separation. Clustered and cluster percolated states consistently exhibit an intermediate range order peak in their structure factors with a magnitude above 2.7, leading to a semi-empirical rule for identifying clustered fluids in scattering experiments.

Introduction

Modern liquid state theory and colloid science employ computer simulations and the methods of statistical mechanics to quantitatively predict the phase behavior of a broad range of simple fluids and colloidal dispersions with widely varying inter-particle interactions. This is critical for *a priori* design of materials with specific properties for functionality ranging from food products[1,2] to injectable biopharmaceuticals based on concentrated monoclonal antibody solutions.[3] Colloidal and molecular fluids are often accurately represented by a combination of long range attraction and short range repulsion.[4,5] The basic understanding of such fluids can be traced back to the work of van der Waals,[6] where the interplay between excluded volume and long-range attraction leads to gas–liquid critical points, and if the system is low in polydispersity, crystallization and a triple point.[7–9] More recently, the soft matter community has focused attention on systems with an excluded volume with short-range attraction (SA) and long-range repulsion (LR), or SALR potentials. These systems are of particular interest as they can produce liquid states comprised of equilibrium clusters.[10–17] These complex potentials are pertinent to fundamental scientific research as well as many industrially relevant materials, such as protein solutions. Therefore, efforts are being made to understand the more complicated phase behavior arising from the interplay of both potential features.[12,13,18]

In contrast to irreversible fractal aggregates, or flocs, clusters in an SALR system can be reversible aggregates with a preferred finite size.[18,19] Attraction induces particle aggregation, which continues until the cluster accrues a sufficiently strong repulsion to prevent further growth. One important difference between flocs and these types of clusters is their lifetime. Floc size grows continuously in the reaction- or diffusion-limited regimes until forming a system spanning aggregate or settling out of solution.[20,21] In contrast, clusters in an SALR system can have a thermodynamically preferred size distribution and particles within the clusters have a finite rate of exchange with particles in the bulk. Recent experimental studies distinguish clusters as transient, dynamic, or permanent according to their dynamics.[22,23]

Systems with an SALR potential exhibit a variety of distinct microstructural states. In addition to stable clustered fluids, aggregation of such clusters have been reported as precursors or building blocks of gels.[11–15,24] Both simulations and theoretical calculations also indicate the possibility of forming Wigner crystals of mutually repulsive clusters at low temperature.[13,19] A

[a]*Center for Neutron Science, Department of Chemical and Biomolecular Engineering, University of Delaware, 150 Academy St, Newark, DE 19716, USA. E-mail: yun.liu@nist.gov; wagnernj@udel.edu*

[b]*División de Ciencias e Ingenierías, Universidad de Guanajuato, Loma del Bosque 103, 37150 Leon, Mexico*

[c]*NIST Center for Neutron Science, National Institute of Standards and Technology, Gaithersburg, MD 20899, USA*

† Electronic supplementary information (ESI) available: Pertinent details of the results discussed throughout the text are provided for further understanding. All potentials are plotted together for comparing the relative range and strength of attraction and repulsion. Details of effective range of attraction calculations are shown along with corresponding reduced second virial coefficients for comparison with previous results. Finally, additional pertinent details are provided regarding of the effect of the range of repulsion on the applicability of the generalized state diagram. See DOI: 10.1039/c3sm53220h

large variety of additional cluster-based arrested states have also been reported in SALR systems with a very strong, very long range repulsion.[25] Recent work has corroborated these results by explicitly demonstrating a shift in the percolation transition to smaller volume fractions with increasing strength of repulsion.[26] Note that the range of attraction has a strong effect on the phase behavior of systems with competing interactions. Works focusing on systems with repulsion and long-ranged attraction, about the size of a particle diameter, display distinctly different phase transitions at low temperature compared to SALR systems.[27–29] As the attractive range for most cluster forming experimental systems is very short, unless explicitly mentioned, the discussion in the rest of the paper will only focus on cases where the range of SA is around 10% of a particle diameter or shorter.

Clarification of the phase behavior of clustering solutions is of significant technological importance for biological materials of varying complexity, ranging from model globular proteins to therapeutic monoclonal antibodies (mAbs). Recent experimental work with high concentration solutions of mAbs[30–35] and globular proteins, such as lysozyme,[10,15–17,22,36] suggest extensive formation of clusters in solution (not necessarily of a preferred size). In particular, clustering of mAbs has been shown to have a strong effect on solution viscosity depending on the type of clusters formed[32,35] However, the fundamental issue of experimentally identifying clustered fluids in protein solutions is still debated in literature,[10,16,17,22,37–39] which further complicates the matter.

Early small angle X-ray and neutron scattering studies of lysozyme protein[10,39] identified a unique peak at small scattering wave vectors, or q-values. This low-q peak was thought to be due to cluster formation and hence, termed the "cluster peak".[10] Simulations and integral equation theory calculations have determined the dependence of the low-q peak position and magnitude on SALR potential parameters.[37,40,41] Cluster states estimated in this way have been mapped onto a reduced temperature–density phase diagram.[15,42] However, recent experimental studies[17,23] and simulations[24] have provided direct evidence that low-q peaks are not necessarily a consequence of clustering as envisioned in the earlier sense, but rather, are a general representation of the presence of intermediate range order (IRO) in the fluid. Hence, a low-q peak in the structure factor is not an accurate indication of cluster formation and is more accurately termed an IRO peak. Therefore, clustered fluid states in SALR systems based on this misidentification are inaccurate.[24]

This contribution builds upon a previous attempt to study the phase behavior of SALR systems that provided state definitions and identified a possible link between the existence of clustered fluid states and the gas–liquid phase behavior of a reference potential fluid.[24] In that work, clustered states were found to exist in the two-phase region of the liquid state phase diagram of an appropriately defined reference fluid with excluded volume and a short range attraction. As the attractive interactions drive cluster formation, it is not surprising in hindsight that an appropriately defined reference attractive system can provide physical insight and quantitative guidance into the phase space occupied by various structural states of the SALR fluid. However, the transition boundary from dispersed fluid states to clustered states was not precisely determined, but was compared with the binodal line of the reference potential fluid. Here, by investigating a large number of state points and a wide range of potential parameters including published literature results, we conclusively demonstrate the broader generality of this observation.

The concept of corresponding states in thermodynamics is well understood for simple liquids that interact according to a similar underlying interaction potential, such as the classic Leonard-Jones fluid.[43] However, the phase behavior of systems with attractive interactions depends strongly on the range of attraction such that corresponding states does not hold.[8] However, when limiting the range of attraction to less than ~10% of a particle diameter, an extended law of corresponding states (ELCS) for the structure and liquid–liquid binodal was observed by Noro and Frenkel.[44] It was found that the liquid structure and phase behavior is less sensitive to the exact shape of the potential than the total effective strength of attraction. When represented in terms of the normalized second virial coefficient, ELCS has been shown to accurately represent systems interacting by square well and attractive Yukawa potentials with short range attraction.[45–47] Further, ELCS was recently shown to remain accurate for these potentials with a range of attraction as large as 25% of a particle diameter.[47] Therefore, the phase behavior of fluids interacting with a potential composed only of the short range attractive component of a more complex SALR potential will also reduce to a common corresponding states diagram according to ELCS. We propose that the generalized phase behavior of these reference fluids will provide context and physical insight into cluster formation in SALR systems in general, as suggested for a single SALR potential in our earlier work.[24]

Here, we systematically investigate the transition from a dispersed fluid to a clustered fluid by exploring more state points, broadening the space of potential parameters, and examining the effect of different potential shapes, including results reported in literature. From these simulations, we construct a corresponding states diagram for a broad and representative range of SALR potential systems. Simulations are performed utilizing two functional forms of SALR interaction potentials with varying parameters, temperature and volume fraction. We augment recent work by studying a system at a typical range of repulsion equivalent to roughly 2σ.[40,42,48,49] A corresponding states diagram is found for the reference attractive potentials and this is used to create a generalized state diagram for clustered fluids. We have also summarized and included published results[12,13,19] and show that they too are consistent with our proposed generalized, corresponding states phase diagram. Finally, the formation of clustered and cluster percolated states is also shown to correlate well with the magnitude of the IRO peak magnitude as well as the average coordination number of particles in the fluid, providing a new, semi-empirical method for identifying clustered fluids directly from scattering experiments.

Simulation and analysis methods

Simulation protocol

Monte Carlo (MC) computer simulations[50,51] consisting of 1728 particles in the NVT ensemble within the one-phase region, employing periodic boundary conditions, are used to study spherical particles with central force two-body interactions over a wide range of interaction parameters. Starting from a simple cubic lattice, each system is thermalized for 2×10^7 steps. After equilibration, thermodynamic and structural parameters were averaged over 4×10^4 independent configurations. The initial displacement distance of 0.1, where all distances are normalized by the particle diameter σ, is dynamically adjusted to maintain an acceptance ratio of 30%. The observables were averaged over 10 different seeds to reduce the intrinsic uncertainties. System size effects were also monitored in a few cases (data not shown), but in all cases $N = 1728$ particles provided a reasonable system size that allowed us to optimize the computational time.

Particles interact *via* an isotropic pairwise potential with a combination of short range attraction and long range repulsion. A representative potential of each type is shown in Fig. 1. The first type, known as a hard sphere double Yukawa (HSDY) potential, represents attraction and repulsion with an exponential function:

$$\frac{U_{\mathrm{HSDY}}(r)}{kT} = \begin{cases} \infty & r < 1 \\ \left(\dfrac{1}{T^*(1-\lambda)r}\right)\left(-\mathrm{e}^{-z_1(r-1)} + \lambda \mathrm{e}^{-z_2(r-1)}\right) & r \geq 1 \end{cases}, \quad (1)$$

where r is the reduced particle–particle separation, z_1 is the inverse range of attraction, z_2 is the inverse range of repulsion, λ is the ratio of strength of repulsion to attraction, and T^* is the reduced temperature that represents the relative strength of thermal energy and the strength of attraction. Previous integral equation theory calculations have demonstrated the formation of IRO peaks by this potential.[40,42]

We also consider a pairwise potential that combines a hard sphere component with the Leonard-Jones 2α–α form of short range attraction and Yukawa repulsion, called the Leonard-Jones–Yukawa (LJY) interaction potential:

$$\frac{U_{\mathrm{LJY}}(r)}{kT} = \begin{cases} \infty & r < 1 \\ \dfrac{1}{T^*}\left[4\left(r^{-2\alpha} - r^{-\alpha}\right) + A\dfrac{\xi}{r}\mathrm{e}^{-r/\xi}\right] & r \geq 1 \end{cases}, \quad (2)$$

where α is inversely related to the range of attraction, ξ is the range of repulsion, and A is the ratio of strength of repulsion to strength of attraction. This potential has been previously shown to produce clustered and percolated states[12,13] and is representative of attractive interactions arising from dispersion forces.

Protein interactions originate from complex anisotropic charge distributions, upon which the phase behavior is built and has been captured by patchy colloidal models.[52] While not completely representative, protein phase behavior has been successfully modeled by effective isotropic interactions.[47,53] The true functional form of these effective interactions is debated in literature.[54,55] However, inter-protein interactions in lysozyme solutions have been accurately represented by both the HSDY[22,36] and LJY[15,16,56] potentials used in this work.

As a typical representation of the solution structure obtained from scattering experiments, we calculate the radial distribution function, $g(r)$, and structure factor, $S(q)$, for each state. The radial distribution function is calculated by averaging all particle configurations using direct summation according to:

$$g(r) = \frac{V^2}{n^2}\left\langle \sum_{i=1}^{n}\sum_{j=1}^{n}\frac{\delta(r_{ij} - r)}{V}\right\rangle, \quad (3)$$

using standard methods.[50,51] Here, n is the number of particles, V is the sample volume, and δ is the Dirac delta function. Restricting the calculation of eqn (3) to include only particles contained in clusters, and explicitly accounting for each particle within the double summation, generates cluster–cluster correlations defined by $g_{cc}(r)$, the radial distribution function of clustered particles. This function represents the degree of order between clusters and helps in distinguishing between structural states formed by SALR systems. The structure factor is calculated according to its relationship with the radial distribution function:

$$S(q) = 1 + \rho\int_0^\infty \frac{\sin(qr)}{qr}[\mathrm{g}(r) - 1]\,4\pi r^2 \mathrm{d}r, \quad (4)$$

where ρ is the solution density and $q = (4\pi/\lambda)\sin(\theta/2)$ is the wave vector with the incident wavelength, λ, and scattering angle, θ, as parameters. Structure factors and radial distribution functions calculated from all simulations were found to quantitatively agree with numerical calculations using a thermodynamically self-consistent closure relation for the Ornstein–Zernike (OZ) equation.[24,49]

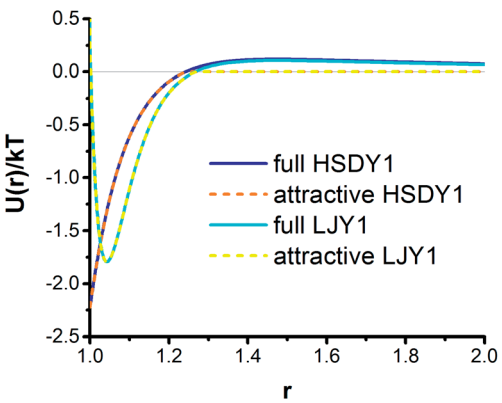

Fig. 1 Representative HSDY and LJY interaction potentials are shown as solid lines (HSDY1 and LJY1 potentials from Table 1). Phase separation, indicated by the binodal, is calculated with respect to the attractive component of the potential (dotted line) termed the reference attractive potential. The cut-off distances used to determine connectivity is defined as the separation distance at which the mixed potential has zero energy.

Reference potential liquid–liquid binodal calculation

A reference potential is defined for the HSDY and LJY potentials as the purely attractive portion of each potential. These are

shown in Fig. 1 as dashed lines with their corresponding "full" potential. The reference potentials are defined for HSDY systems as:

$$\frac{U_{\mathrm{HSDY}}^{\mathrm{ref}}(r)}{kT} = \begin{cases} \infty & r < 1 \\ \left(\dfrac{1}{T^*(1-\lambda)r}\right)\left(-\mathrm{e}^{-z_1(r-1)} + \lambda \mathrm{e}^{-z_2(r-1)}\right) & 1 \le r \le r_c \\ 0 & r > r_c \end{cases}, \tag{5}$$

and for LJY systems as:

$$\frac{U_{\mathrm{LJY}}^{\mathrm{ref}}(r)}{kT} = \begin{cases} \infty & r < 1 \\ \dfrac{1}{T^*}\left[4\left(r^{-2\alpha} - r^{-\alpha}\right) + A\dfrac{\xi}{r}\mathrm{e}^{-r/\xi}\right] & 1 \le r \le r_c \\ 0 & r > r_c \end{cases}, \tag{6}$$

where r_c is the cut-off distance defined as the separation at which the potential produces a zero interaction energy.[24] For consistency, this cut-off distance is also used to determine connectivity. The interaction parameters and corresponding cut-off distance of each of the potentials studied in this work, including those of previous studies used for comparison, are provided in Table 1.

Binodal lines representing liquid–liquid phase separation are generated by discrete perturbation theory (DPT)[57–60] for the reference attractive potentials of each system in Table 1. DPT represents the interaction potential by numerous discrete square well-like steps and is known to calculate accurate gas–liquid binodals and critical points of purely attractive systems.

State definitions

A particle is defined as part of a specific cluster when it is less than a distance r_c from a neighboring particle. These calculations distinguishing particle "species" are summarized by the cluster size distribution, $n(s)$. We normalize the cluster size distribution by the cluster size, s, and system size, N_p:

$$N(s) = \left(\frac{s}{N_p}\right)n(s), \tag{7}$$

similar to that proposed by Stauffer[61] and used by Chen *et al.*[62] While $n(s)$ represents the number of clusters of s particles existing in the system and is biased towards smaller cluster sizes, $N(s)$ represents the fraction of particles contained in clusters of size s and is a normalized function for all cluster sizes. This normalized cluster size distribution defines the state of the fluid at each set of conditions using definitions established in an earlier publication.[24] Fig. 2 shows representative cluster size distributions of each of the four states found in SALR systems: dispersed fluid, clustered fluid, random percolated and cluster percolated states. Representative particle configurations from simulation snapshots of a dispersed and clustered fluid are shown in Fig. 2b and c, respectively, to demonstrate the distinctive structure found in clustered states.

A dispersed fluid is distinguished by a monotonically decreasing $N(s)$, which represents a state where monomers are the most abundant species in the system and clusters form without a preferred size. For comparison, even simple hard

Table 1 The inverse range of attraction, inverse range of repulsion, the relative strength of repulsion to attraction, and the cut-off distance are given for the HSDY potentials (z_1, z_2, λ, and r_c respectively) and for the LJY potentials (a, $1/\xi$, A, and r_c respectively) represented in this work. All potentials plotted relative to each other can be found in the ESI

HSDY #	z_1	z_2	λ	r_c
HSDY 1	10	0.5	0.1	1.2424
HSDY 2	11.3023	0.5	0.094515	1.2184
HSDY 3	11.9279	0.5	0.092307	1.2085
HSDY 4	8.134	0.5	0.2	1.2108
HSDY 5	20	0.5	0.175	1.0894
HSDY 6	5	0.5	0.2	1.3577
[40]HSDY 7	10	0.5	0.01	1.4847
[40]HSDY 8	10	0.5	0.05	1.3153
LJY #	a	$1/\xi$	A	r_c
LJY 1	16.6755	0.5	0.090982	1.2665
LJY 2	32	0.5	0.17	1.1005
[13]LJY 3	100	0.5	0.2	1.0282
[19]LJY 4	100	0.5	0.05	1.0433
[12]LJY 5	18	2.0	8	1.1358

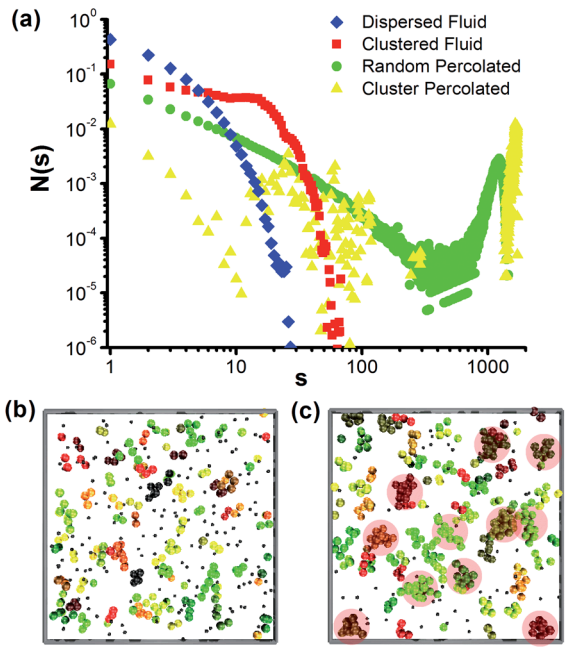

Fig. 2 (a) Characteristic cluster size distributions are shown for each of the four states formed in SALR systems (specifically in potential HSDY1), which are used to define the state of each condition of volume fraction and temperature. Shown are a dispersed fluid ($\phi = 0.05$, $T^* = 0.46$), clustered fluid ($\phi = 0.05$, $T^* = 0.25$), random percolated ($\phi = 0.15$, $T^* = 0.46$) and cluster percolated ($\phi = 0.15$, $T^* = 0.25$) state. While the difference in percolated structures has been highlighted previously,[24] a representative configuration of a dispersed fluid (b) and a clustered fluid (c) are compared to demonstrate the unique structure of clustered states. Each cluster is given a different color and monomers are made smaller for clarity. Clusters in the preferred size region ($8 \le s \le 15$) of the clustered state are highlighted in red.

sphere fluids show a similar monotonically decaying cluster size distribution at finite concentration.[24] Note that many clustered states defined by previous studies, which have been defined by an average cluster size of 2 or greater[15,63] or a large effective hydrodynamic radius,[17] will be labeled as dispersed fluid states under this definition. Although dispersed fluids are "monomer-dominated" they will still contain some clusters (as is even observed for hard sphere fluids).

The formation of a local maximum in $N(s)$ for $s > 1$ is used to define a clustered fluid state. Under these conditions the ensemble average contains a range of cluster sizes that are energetically preferred over others. Unlike dispersed fluids that contain contributions from all cluster sizes, clustered fluid properties are expected to be governed predominantly by clusters around the preferred size. This strict taxonomy, combined with an appropriate definition of r_c, provides consistency and physical significance to the solution structure and its correlation with both the particle interactions and mechanical properties of the material.

A prerequisite of gelled or glassy states is the formation of percolated clusters.[64,65] Percolation is defined according to the conventional method when at least 50% of the sampled configurations in the simulation trajectory contain a system-spanning cluster.[66] Under these circumstances, the cluster is effectively infinite when applying periodic boundary conditions. Typical percolating fluids exhibit a single peak in the $N(s)$ comparable to the system size and these states are denoted as random percolated.[67] Clustered states will also percolate upon concentration and their $N(s)$ will exhibit both the cluster peak as well as the system-size peak, as shown in Fig. 2a. This is a distinctly different structural state from percolation in the dispersed fluid as there is a preferred size for the "building blocks" that comprise the percolation cluster. Further demarcation of these two distinct percolated states can be accomplished by analyzing their structural order as shown in a previous study.[24]

In the following, between 5 and 15 state points are chosen for each potential and associated with one of the four states (dispersed fluid, clustered fluid, random percolated or cluster percolated). These states are then located on a corresponding states phase diagram relative to the predicted binodal of a corresponding reference attractive fluid.

Results and discussion

Generalized corresponding states diagram

Table 1 shows the potential parameters studied in this work. The choice of parameters is motivated by research that models physically meaningful systems observed in experiments and also overlap with potential parameters studied in literature. This range is extensive and covers many physically realizable systems of interest to the protein, biopharmaceutical, nanoparticle, and colloid communities.

As a representation of the diversity in interaction potentials used in this study, a selection of reference attractive potentials and their corresponding binodals are plotted together in Fig. 3a (only half are shown for the sake of clarity). Critical points are found to vary in volume fraction from roughly 0.2 to 0.4 while critical temperatures vary from about 0.15 to 0.55. In accordance with previous work,[47] as the total attractive strength decreases, either by a smaller range or weaker strength of attraction, the corresponding binodal has a smaller value of T_c^*. However, potentials HSDY5 and LJY4 appear to deviate from this trend. If the range of attraction is too short, Asakura–Oosawa and attractive Yukawa potentials have been shown previously to bias the liquid branch of the binodal,[47] as observed in Fig. 3a for potentials HSDY5 and LJY4.

The binodals of all reference attractive potentials are plotted together in Fig. 3b in a corresponding states plot by reducing the temperature and volume fraction by the critical values. Excellent agreement is observed. The uncertainty is greatest in the calculations for potentials HSDY5, LJY3, and LJY4, which show the largest deviations from the average behavior. DPT calculations become more difficult for potentials with ranges of attraction less than 1.1σ, or less than 10%, and deviations from exact behavior have been reported to be as large as 15%.[60] In what follows, the binodal of potential HSDY1 is used for reference as representative of all these systems. The critical

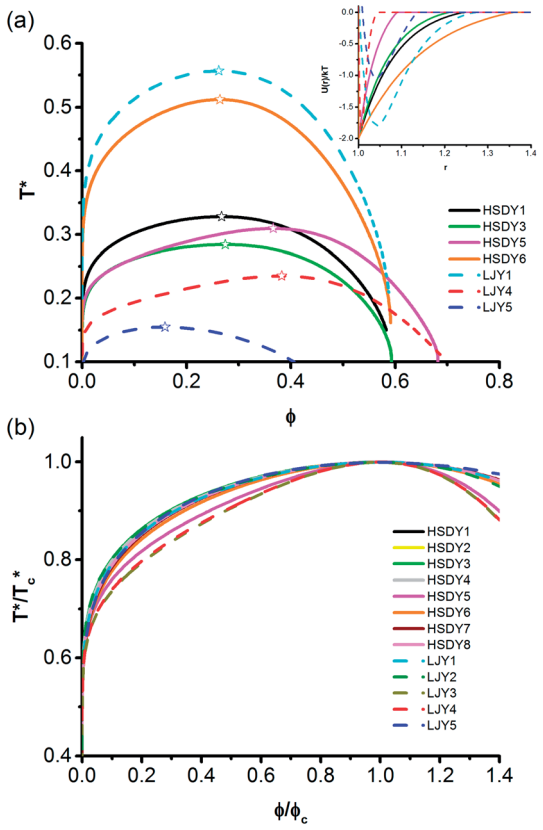

Fig. 3 (a) Binodals corresponding to the reference attractive potentials for 7 of the 13 SALR potentials studied in this work are plotted together. The inset displays the associated reference attractive potential of each binodal with the same line color and style. (b) Binodal lines of the reference attractive potential of all systems studied are normalized by their respective critical points and shown to overlap. Three potentials (HSDY5, LJY3, and LJY4) do not overlap entirely; however, their state points still follow the trends shown in this work.

behaviors of these reference fluids are consistent with those reported for square well[45] and attractive Yukawa[46] fluids, shown in the ESI.†

Equilibrated fluid structures are calculated for the potentials given in Table 1 and the state points presented in Fig. 4. Fig. 4 is a master corresponding states diagram using the critical point (ϕ, T_c^*) of the reference attractive fluid. After this normalization the four types of states are observed to lie in defined regions of the state diagram (distinguished by color) relative to the reference attractive fluid binodal. As might be expected, dispersed fluids and random percolated states lie above the binodal of the reference attractive fluid at low and high volume fractions, respectively. Similarly, clustered fluids and cluster percolated states lie within the two-phase region of the reference attractive fluid.

These results indicate that the binodal of a reference attractive potential is an accurate indicator of the location of clustered states and cluster percolated states in the phase space of SALR systems. This confirms our earlier observation and extends it to a much broader range of potential parameters. The overlap of the dispersed and clustered fluid regions is representative of the uncertainty in the binodals calculated by DPT. In the absence of repulsion, below the reference binodal the fluid would phase separate, which suggests cluster formation in the presence of a long range inter-particle repulsion corresponds to a frustrated phase separation. The long range repulsion provides a balancing force that prevents unbounded growth of clusters driven by a strong attractive driving force, resulting in clusters with a preferred size. Increasing volume fraction leads to the formation of more clusters of the preferred size until they merge and percolate the system volume, producing a percolated network with strong intermediate range order. The observation of a corresponding states diagram for cluster fluids provides an efficient and robust method for estimating the conditions of cluster formation for a wide range of fluids.

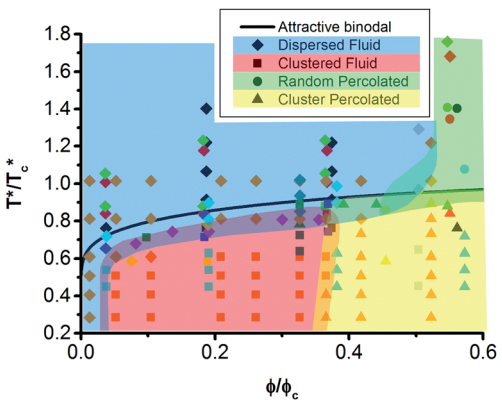

Fig. 4 Generalized phase diagram for clustered states. State points for the interaction potentials studied in this work are combined with results from ref. 13, 19, and 12 (orange, dark cyan, and grey points, respectively). The various potentials used are shown in the ESI† where the colors of the points correspond with the potential used in those simulations. Four distinct regions are found to exist when normalized by their respective reference attractive potential critical points: dispersed (blue), clustered (red), random percolated (green), and cluster percolated (yellow). The clustered and cluster percolated states exist only within the liquid–liquid phase separation region of the reference attractive potential indicating an arrested phase separation that leads to states comprised of clusters of a preferred size.

Heuristic models for identifying clustered states

All four of the state classifications explored here have previously been demonstrated to produce IRO peaks in simulations and scattering experiments. Therefore, these peaks in scattering experiments are in and of themselves insufficient to indicate the formation of clustered or cluster percolated states. However, previous literature reports indicate, but do not elaborate on, a possible correlation between the magnitude of IRO peaks and the formation of clustered states as defined here (*i.e.*, a peak in the cluster size distribution).[12,19] Such a correlation is logical as a high peak magnitude indicates greater structure in the fluid, which would be expected if a preferred cluster size is evident. Fig. 5 shows the magnitude of the IRO peak for all states explored in this work. An IRO peak magnitude of ~2.7 consistently identifies a transition from dispersed fluid and random percolated states at smaller magnitudes to clustered fluid and cluster percolated states at larger magnitudes, respectively. Fig. 5 also includes data from literature[12,19] shown as open and half-filled systems that also follow this semi-empirical observation. Correspondingly, experimental studies of lysozyme protein solutions with a broad cluster size distribution, *i.e.*, a dispersed fluid as defined here, indeed form IRO peaks whose magnitude remain below 2.7.[15]

Fig. 5 also indicates that clustered and cluster percolated states can form IRO peaks with a magnitude of 10 or greater. According to the work of Hansen and Verlet,[68,69] the evolution of a peak in the structure factor with a magnitude greater than 2.85 is indicative of a freezing transition. The formation of Wigner crystals in cluster fluids has been demonstrated by proposed simple models.[19] Previous work has shown the empirical

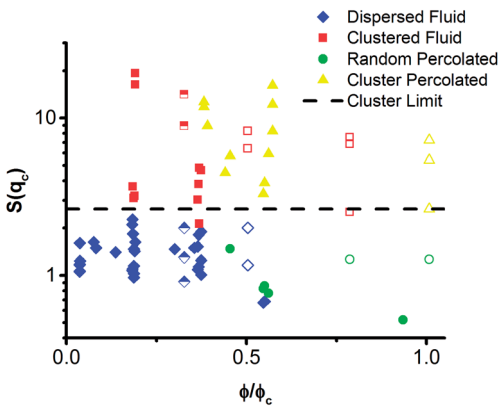

Fig. 5 IRO peak magnitudes plotted against the reduced volume fraction. Clustered and cluster percolated states have a magnitude above an apparent critical magnitude of ~2.7 while monomer and monomer percolated states form IRO peaks with magnitudes below this value. Filled symbols are from this work, open symbols are taken from ref. 12, and half-filled symbols are from ref. 19.

Hansen–Verlet criteria to accurately predict phase transitions for the HSDY interaction potential.[70] However, this work also demonstrates that for short range attraction ($z_1 \geq 8$) as used in the current simulations, these systems are expected to remain in a fluid state. In agreement with these expectations, we find no evidence of crystallization in our simulations, most likely due to the degree of polydispersity of cluster sizes and shapes in cluster percolated and clustered states.

Finally, we note another semi-empirical criterion for the transition between states as given by the average particle coordination number, shown in Fig. 6. Specifically, the transition occurs at an average coordination number of ~2.4 from a dispersed fluid state to either a clustered state or random percolated state. (Note that the transition coordination number from a random percolated state to a cluster percolated state is larger than 2.4). This minimum coordination number has been reported as a criterion for dynamically arrested states in numerous atomic systems[71] and recently has also been observed in colloidal systems.[65] Theory and experimental studies of atomic glasses suggest that short range attractive fluids require, on average, at least 2.4 neighbors in order to produce what is known as "rigidity percolation." This phase transition is based theoretically on the minimum number of neighbors or caging elements required to restrict the degrees of freedom available to particles in three dimensions.[71] For systems that can be directly imaged by optical microscopy, this criterion for the formation of clustered states will be more easily accessible than the magnitude of the IRO peak in scattering.

Although expected for random percolation, the applicability of this average bond number criterion to also predict cluster fluid formation is unexpected. The formation of high magnitude IRO peaks provides a possible clarification as to why this criterion holds. Such strong intermediate range order indicates a large degree of localization that should inevitably hinder the motion of particles and clusters associated with caging. Due to the long ranged nature of inter-particle and inter-cluster repulsion, caging is possible over intermediate range rather than the particle length scale as found in glassy and percolated states for fluids interacting only with short range attraction. In fact, by using mode-coupling theory, the formation of a cluster glass has been predicted when the magnitude of the IRO peak is very large.[72] Particles within a cluster are caged in the traditional sense by many neighbors. Thus, clusters likely have locally glassy structures (*i.e.*, amorphous with limited mobility) that is sustained by a minimum average coordination number. Neutron spin echo studies of lysozyme diffusivity appear to corroborate this hypothesis.[15,17,23] The observation that collective diffusivity is q-independent at high q-values indicates that the dynamics are dominated by cluster diffusivity, suggesting that local dynamics are slow and possibly glassy in nature.

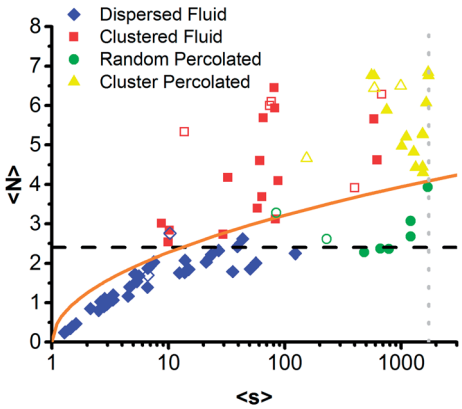

Fig. 6 Average coordination number $\langle N \rangle$ as a function of average cluster size $\langle s \rangle$. Clustered, random percolated, and cluster percolated states all exist above the "critical" value of $\langle N \rangle = 2.4$ necessary for rigidity percolated.[73] Eqn (8), which shows the extent of local order within clusters, separates dispersed fluids and random percolated states from clustered and cluster percolated states. Filled symbols are from this work and open symbols are taken from ref. 12.

Examining the clusters evident in our simulations, we find an empirical relationship between the average cluster size and minimum average coordination number (*i.e.*, number of nearest neighbors) required to form clustered states. This correlation, shown in Fig. 6, is based on all state points studied in this work as well as those from a previous study:[12]

$$\langle N \rangle = 1.5(\ln \langle s \rangle)^{0.5}, \quad (8)$$

where $\langle N \rangle$ is the average coordination number and $\langle s \rangle$ is the average cluster size. As clusters grow in size, more particles are contained within the cluster, and thus have a higher coordination number, as compared to those at the cluster surface or free in solution. However, this minimum average coordination number is indicative of the local order necessary for cluster formation to be energetically preferred. A larger coordination number produces an enthalpic contribution to the free energy that compensates for the reduction in entropy in the compact structure. The net free energy is thus lowered for cluster sizes around the average, making them preferential to other sized clusters.

As a measure of this minimum extent of local order, we compare the average coordination number needed for cluster formation calculated by eqn (8) with that calculated numerically for spherical clusters of s particles with face-centered, body-centered, simple cubic and diamond cubic lattices (FCC, BCC, SC and DC, respectively). Based on the well-known packing fraction of each of these lattices (0.74, 0.68, 0.52 and 0.34, respectively) and the direct (non-linear) correlation between coordination number and volume fraction, we can estimate the local volume fraction of clusters formed in clustered states. Fig. 7a shows the trends in coordination number with cluster size for all four lattices explored as well as along the empirical cluster line, eqn (8). Normalizing the cluster line by each of the four crystal structures provides remarkably flat lines, indicating a consistent relationship between local packing fraction and coordination number regardless of cluster size. These coordination number ratios (N_{clus}/N_{crys}) are plotted as a function of the difference in volume fraction from the maximum possible packing ($\phi_{FCC} = 0.74$) in Fig. 7b to provide a linear fit. The equivalence point calculation produces an estimation of *local* volume fraction for cluster formation at 0.38 ± 0.04. Previous

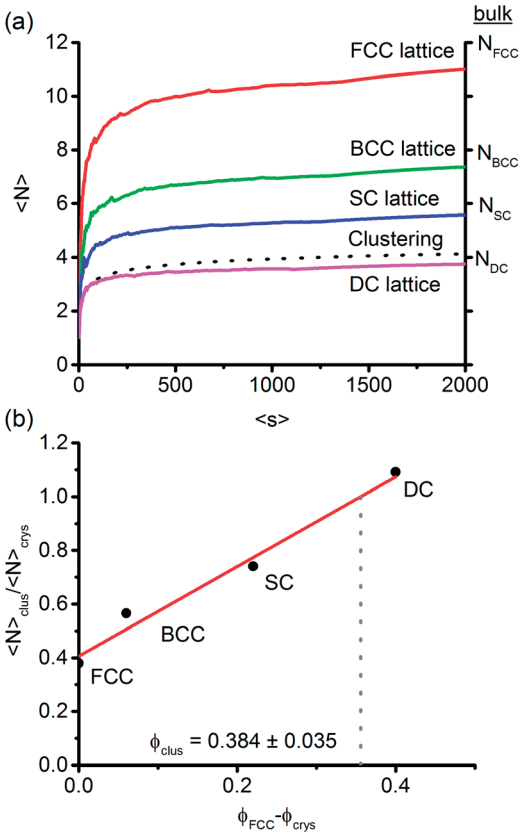

Fig. 7 (a) The average coordination number as a function of cluster size is compared for the cluster transition represented by eqn (8) and spherical clusters with four different crystal lattices. All crystal structure coordination numbers approach their bulk values in the limit of large clusters. (b) Normalizing the cluster coordination number by that of the four crystal lattices produces constant values that are plotted as a function of the corresponding crystal volume fraction relative to maximum packing, which is the FCC lattice. The linear correlation is used to calculate the equivalence point of the coordination numbers and estimate the minimum volume fraction needed to form clustered states at 0.384 ± 0.035.

experimental work by Campbell *et al.* provides a strikingly similar value for the local packing fraction of clusters of ~0.42 at all bulk volume fractions in which clustering was observed.[11]

Bomont *et al.* identified a possible signature of cluster formation as a jump in the excess entropy, s^{ex}, of SALR potential systems.[48] However, the jump was associated with the initial presence of an IRO peak rather than a peak in $N(s)$, as used in this work to define clustered states. Their work utilized the same parameters as potential HSDY1 employed here, which we show to form clustered states below the reference attractive binodal, or below a T^*/T_c^* of roughly 0.8 ($T_c^* = 0.328$). The jump observed in s^{ex} occurred at a T^* of 0.688, far above the reference attractive binodal. Therefore, this jump is likely a signature of the entropy change related to intermediate range order rather than explicitly with the formation of clustered states. However, further study of possible thermodynamic signatures of cluster states would greatly progress our understanding of these unique systems and our capability of experimentally identifying their formation.

Role of long-range repulsion

During our study, we have fixed the range of the repulsion to be about 2σ ($z_2 = 0.5$) and conclusively demonstrated the existence of corresponding states of colloidal systems with an SALR potential. If the range of repulsion becomes even longer ranged, SALR systems are expected to still favor the formation of finite size clusters. We speculate that the proposed corresponding states diagram will remain valid, though future works are needed to demonstrate this. However, when the range of repulsion becomes shorter, the formation of small clusters may not be energetically favorable. Thus, this could pose a limit of our method to identify the cluster states having clusters with a preferred size.

Here, we explore the effect of the range of repulsion in the HSDY1 potential by studying one clustered state point with $\phi = 0.05$ and $T^* = 0.25$. The full study of all state points is beyond the scope of this paper and will be addressed in future works. The resultant states at this volume fraction and temperature are analyzed as a function of the range of repulsion by varying z_2 both above and below the value of 0.5 originally used.

The variation of the repulsion range is performed while maintaining the reduced second virial coefficient of the attractive portion of the potential and the point of zero energy (*i.e.*, the cut-off distance defining connectivity). This is accomplished by also shifting the range of attraction, z_1, and strength of repulsion, λ, which consequently varies the maximum strength of repulsion. By maintaining constant B_{2c}^* values, all these new states share the same reference binodal. When decreasing the range of repulsion by increasing z_2 above roughly 0.8, the clustered states are observed to transition to dispersed fluid states as shown in Fig. S6 in the ESI.† Note that our simulation results show that this state point remains in the one phase region below a z_2 of roughly 2.5.

The disappearance of clustered states with significant decrease in the range of the repulsion is due to the fact that small cluster formation is no longer energetically favorable. This can be estimated by some simple calculations as demonstrated in Fig. S5 in the ESI.† Following previous work,[18,19] we calculate the configuration energy per particle at the ground state for a single cluster for a large set of HSDY interaction parameters. Conditions producing an energy minimum as a function of cluster size are considered capable of producing clusters. As shown previously for an LJY potential,[18] both increasing and decreasing the strength and range of repulsion too significantly will destabilize the formation of clusters of a preferred size. Under the specific scenario where the strength and range of repulsion are too small, insufficient repulsion exists to stabilize clusters to a finite size, leading to unstable aggregation. Therefore, above a z_2 value of 0.8, clusters are not preferred in this limit of infinite dilution as shown in Fig. S6 in the ESI.† At finite temperatures and volume fractions, entropic contributions to the system free energy will only further destabilize cluster formation. Therefore, this simple model provides a limit of the generalized state diagram applicability.

Very interestingly, the transition from clustered to dispersed fluid states with decreasing range of repulsion also corresponds

with a shift in IRO peak magnitudes below 2.7 and a shift in average coordination numbers below 2.4, shown in Fig. S8 in the ESI.† Therefore, the semi-empirical observations of the IRO peak in the small angle scattering exceeding ~2.7 in magnitude and of the average coordination number exceeding 2.4 seem to be very robust signatures of a clustered fluid.

We also note that if the strength of the repulsion is very large, relatively short ranges of repulsion may still favor the formation of finite size clusters. Therefore, the upper limit of z_2, above which clusters with a preferred size no longer form, may shift to larger values. Our preliminary study indicates that when $\lambda \approx 1$, z_2 could be larger than 1.6. Interestingly, even though there may not be a cluster state with an optimal size when the range of the repulsion is too short, there is still an interesting phase region sandwiched between the binodal lines of the reference potential and the full SALR potential. There may be some other interesting properties of the solutions within this phase region that can also show the behavior of the generalized corresponding states similar to what we have proposed here; however, this is a subject for future investigation.

Conclusions

The main conclusion of this work is the existence of a generalized corresponding states phase diagram for systems with physically meaningful potentials comprised of excluded volume with short range attraction and long range repulsion (SALR). Four distinct types of states are distinguished as dispersed fluid, clustered fluid, random percolated, and cluster percolated states. Most significantly, cluster fluids are located within the binodal of the reference system and in the one-phase region of the HSDY system. This supports the intuitive notion that cluster fluids are what otherwise would be phase separated fluids that are frustrated by the repulsive interactions. This work builds upon and further extends the extended law of corresponding states as proposed for systems with excluded volume and short range attraction by Noro and Frenkel[44] to include this new and technologically important state of clustered fluids.

The defining observation proven by direct simulation is that the phase behavior of a broad range of physically meaningful SALR systems collapses onto a single state diagram when normalized by the critical point of an appropriately defined reference system. The reference system's potential is comprised of the excluded volume and short range attraction of the corresponding SALR potential. Importantly, the liquid state binodals for these reference potentials are very similar and follow the extended law of corresponding states themselves.

All four types of states formed in SALR systems are found in distinct regions of the phase diagram. Of particular importance is the separation of dispersed fluid and random percolated states from clustered fluid and cluster percolated states by the reference attractive binodal. As calculations of the binodal for fluids with attractive potentials are inexpensive, this corresponding state diagram is a very efficient method for estimating the conditions conducive for cluster states. We also provide evidence that the reference attractive binodal is an accurate indication of cluster formation for physically meaningful ranges of repulsion.

A detailed analysis of the structure of clustered fluids provides three semi-empirical criteria necessary for cluster formation in fluids with SALR interactions. The magnitude of the IRO peak for clustered fluids is $\geq$2.7. Further, the average coordination number at the transition from a dispersed fluid to a clustered fluid is observed to be 2.4, consistent with rigidity percolation.[65,73] Finally, the estimated local volume fraction for cluster formation is found to be 0.38 ± 0.04 that is consistent with literature results.[11]

These results demonstrating a generalized phase diagram for cluster formation and the associated semi-empirical properties of clustered fluids offer substantial guidance for the future study of clustered states, which have become an important topic in numerous industries, such as biopharmaceuticals. In particular, these provide methods to rapidly estimate the conditions necessary for cluster formation as well as guidance for identifying possible cluster fluids by scattering and microscopy. Further, simulation and experimental studies of cluster fluid properties and dynamics will also be important for further understanding these intriguing, complex fluids.

Acknowledgements

This manuscript was prepared under cooperative agreements 70NANB12H239 and 70NANB10H256 from NIST, U.S. Department of Commerce. The statements, findings, conclusions and recommendations are those of the author(s) and do not necessarily reflect the view of NIST or the U.S. Department of Commerce. This work has also been supported in part by NSF-Conacyt grant 147892/2011.

Notes and references

1 R. Mezzenga, P. Schurtenberger, A. Burbidge and M. Michel, *Nat. Mater.*, 2005, **4**, 729–740.
2 T. Gibaud, N. Mahmoudi, J. Oberdisse, P. Lindner, J. S. Pedersen, C. L. P. Oliveira, A. Stradner and P. Schurtenberger, *Faraday Discuss.*, 2012, **158**, 267.
3 E. J. Yearley, I. E. Zarraga, S. J. Shire, T. M. Scherer, Y. Gokarn, N. J. Wagner and Y. Liu, *Biophys. J.*, 2013, **105**, 720–731.
4 B. Derjaguin, *Trans. Faraday Soc.*, 1940, **35**, 203–215.
5 E. J. W. Verwey and J. T. G. Overbeek, *Theory of the stability of lyophobic colloids*, Elsevier, 1948.
6 J. D. van der Waals, *On the continuity of the gas and liquid state*, Ph.D. Thesis, Leiden University, 1873.
7 V. J. Anderson and H. N. W. Lekkerkerker, *Nature*, 2002, **416**, 811–815.
8 G. Foffi, G. McCullagh, A. Lawlor, E. Zaccarelli, K. Dawson, F. Sciortino, P. Tartaglia, D. Pini and G. Stell, *Phys. Rev. E: Stat., Nonlinear, Soft Matter Phys.*, 2002, **65**, 031407.
9 M. Miller and D. Frenkel, *J. Chem. Phys.*, 2004, **121**, 535.
10 A. Stradner, H. Sedgwick, F. Cardinaux, W. C. K. Poon, S. U. Egelhaaf and P. Schurtenberger, *Nature*, 2004, **432**, 492.
11 A. Campbell, V. Anderson, J. S. van Duijneveldt and P. Bartlett, *Phys. Rev. Lett.*, 2005, **94**, 1.

12 F. Sciortino, P. Tartaglia and E. Zaccarelli, *J. Phys. Chem. B*, 2005, **109**, 21942.
13 J. C. F. Toledano, F. Sciortino and E. Zaccarelli, *Soft Matter*, 2009, **5**, 2390.
14 H. Sedgwick, S. U. Egelhaaf and W. C. K. Poon, *J. Phys.: Condens. Matter*, 2004, **16**, S4913–S4922.
15 F. Cardinaux, E. Zaccarelli, A. Stradner, S. Bucciarelli, B. Farago, S. U. Egelhaaf, F. Sciortino and P. Schurtenberger, *J. Phys. Chem. B*, 2011, **115**, 7227.
16 F. Cardinaux, A. Stradner, P. Schurtenberger, F. Sciortino and E. Zaccarelli, *Europhys. Lett.*, 2007, **77**, 48004.
17 L. Porcar, P. Falus, W.-R. Chen, A. Faraone, E. Fratini, K. Hong, P. Baglioni and Y. Liu, *J. Phys. Chem. Lett.*, 2010, **1**, 126.
18 S. Mossa, F. Sciortino, P. Tartaglia and E. Zaccarelli, *Langmuir*, 2004, **20**, 10756–10763.
19 F. Sciortino, S. Mossa, E. Zaccarelli and P. Tartaglia, *Phys. Rev. Lett.*, 2004, **93**, 5.
20 P. Meakin, *Phys. Rev. Lett.*, 1983, **51**, 1119.
21 M. Y. Lin, H. M. Lindsay, D. A. Weitz, R. C. Ball, R. Klein and P. Meakin, *Nature*, 1989, **339**, 360.
22 Y. Liu, L. Porcar, J. Chen, W. Chen, P. Falus, A. Faraone, E. Fratini, K. Hong and P. Baglioni, *J. Phys. Chem. B*, 2011, **115**, 7238.
23 P. Falus, L. Porcar, E. Fratini, W.-R. Chen, A. Faraone, K. Hong, P. Baglioni and Y. Liu, *J. Phys.: Condens. Matter*, 2012, **24**, 064114.
24 P. D. Godfrin, R. Castañeda-Priego, Y. Liu and N. J. Wagner, *J. Chem. Phys.*, 2013, **139**, 154904.
25 C. L. Klix, C. P. Royall and H. Tanaka, *Phys. Rev. Lett.*, 2010, **104**, 165702.
26 N. E. Valadez-Pérez, R. Castañeda-Priego and Y. Liu, *RSC Adv.*, 2013, **3**, 25110.
27 D. Pini, G. Jialin, A. Parola and L. Reatto, *Chem. Phys. Lett.*, 2000, **327**, 209–215.
28 A. J. Archer and N. Wilding, *Phys. Rev. E: Stat., Nonlinear, Soft Matter Phys.*, 2007, **76**, 1–14.
29 A. Ciach, *Mol. Phys.*, 2011, **109**, 1101–1119.
30 W. G. Lilyestrom, S. Yadav, S. J. Shire and T. M. Scherer, *J. Phys. Chem. B*, 2013, **117**, 6373–6384.
31 I. E. Zarraga, R. Taing, J. Zarzar, J. Luoma, J. Hsiung and A. Patel, *J. Pharm. Sci.*, 2013, **102**, 2538–2549.
32 K. P. Johnston, J. A. Maynard, T. M. Truskett, A. U. Borwankar, M. A. Miller, B. K. Wilson, A. K. Dinin, T. A. Khan and K. J. Kaczorowski, *ACS Nano*, 2012, **6**, 1357.
33 J. A. Pathak, R. R. Sologuren and R. Narwal, *Biophys. J.*, 2013, **104**, 1–11.
34 A. U. Borwankar, A. K. Dinin, J. R. Laber, A. Twu, B. K. Wilson, J. a. Maynard, T. M. Truskett and K. P. Johnston, *Soft Matter*, 2013, **9**, 1766.
35 E. J. Yearley, P. D. Godfrin, T. Perevozchikova, H. Zhang, P. Falus, L. Porcar, M. Nagao, J. Curtis, P. Gawande, R. Taing, I. E. Zarraga, N. J. Wagner and Y. Liu, *Biophys. J.*, 2014, **106**, 1763–1770.
36 S.-H. Chen, M. Broccio, Y. Liu, E. Fratini and P. Baglioni, *J. Appl. Crystallogr.*, 2007, **40**, s321–s326.
37 Y. Liu, W.-R. Chen and S.-H. Chen, *J. Chem. Phys.*, 2005, **122**, 44507.
38 A. Shukla, E. Mylonas, E. Di Cola, S. Finet, P. Timmins, T. Narayanan and D. I. Svergun, *Proc. Natl. Acad. Sci. U. S. A.*, 2008, **105**, 5075–5080.
39 A. Stradner, F. Cardinaux and P. Schurtenberger, *J. Phys. Chem. B*, 2006, **110**, 21222–21231.
40 J.-M. Bomont, J.-L. Bretonnet and D. Costa, *J. Chem. Phys.*, 2010, **132**, 184508.
41 M. Broccio, D. Costa, Y. Liu and S.-H. Chen, *J. Chem. Phys.*, 2006, **124**, 084501.
42 D. Costa, C. Caccamo, J.-M. Bomont and J.-L. Bretonnet, *Mol. Phys.*, 2011, **109**, 2845–2853.
43 S. I. Sandler, *Chemical, Biochemical, and Engineering Thermodynamics*, 2006.
44 M. G. Noro and D. Frenkel, *J. Chem. Phys.*, 2000, **113**, 2941.
45 J. Largo, M. A. Miller and F. Sciortino, *J. Chem. Phys.*, 2008, **128**, 134513.
46 P. Orea, C. Tapia-Medina, D. Pini and A. Reiner, *J. Chem. Phys.*, 2010, **132**, 114108.
47 N. E. Valadez-Pérez, A. L. Benavides, E. Schöll-Paschinger and R. Castañeda-Priego, *J. Chem. Phys.*, 2012, **137**, 084905.
48 J.-M. Bomont, J.-L. Bretonnet, D. Costa and J.-P. Hansen, *J. Chem. Phys.*, 2012, **137**, 011101.
49 J. M. Kim, R. Castañeda-Priego, Y. Liu and N. J. Wagner, *J. Chem. Phys.*, 2011, **134**, 064904.
50 D. Frenkel and B. Smit, *Molecular Simulations: From Algorithms to Applications*, Academic Press, 2002.
51 M. P. Allen and D. J. Tildesley, *Computer Simulation of Liquids*, Oxford University Press, 1987.
52 C. Gögelein, G. Nägele, R. Tuinier, T. Gibaud, A. Stradner and P. Schurtenberger, *J. Chem. Phys.*, 2008, **129**, 085102.
53 M. Muschol and F. Rosenberger, *J. Chem. Phys.*, 1997, **107**, 1953.
54 A. Stradner, F. Cardinaux and P. Schurtenberger, *Phys. Rev. Lett.*, 2006, **96**, 219801.
55 Y. Liu, E. Fratini, P. Baglioni, W.-R. Chen, L. Porcar and S.-H. Chen, *Phys. Rev. Lett.*, 2006, **96**, 219802.
56 M. C. Abramo, C. Caccamo, D. Costa, G. Pellicane, R. Ruberto and U. Wanderlingh, *J. Chem. Phys.*, 2012, **136**, 035103.
57 A. L. Benavides and A. Gil-villegas, *Mol. Phys.*, 1999, **97**, 1225–1232.
58 G. A. Chapela, F. del Río, A. L. Benavides and J. Alejandre, *J. Chem. Phys.*, 2010, **133**, 234107.
59 A. Vidales, A. L. Benavides and A. Gil-villegas, *Mol. Phys.*, 2001, **99**, 703–710.
60 J. Torres-Arenas, L. A. Cervantes, A. L. Benavides, G. A. Chapela and F. del Río, *J. Chem. Phys.*, 2010, **132**, 034501.
61 D. Stauffer, *Phys. Rep.*, 1979, **54**, 1.
62 S.-H. Chen, J. Rouch, F. Sciortino and P. Tartaglia, *J. Phys.: Condens. Matter*, 1994, **6**, 10855–10883.
63 A. Malins, S. R. Williams, J. Eggers, H. Tanaka and C. P. Royall, *J. Non-Cryst. Solids*, 2011, **357**, 760.
64 A. P. R. Eberle, N. J. Wagner and R. Castañeda-Priego, *Phys. Rev. Lett.*, 2011, **106**, 1.

65 N. E. Valadez-Pérez, Y. Liu, A. P. R. Eberle, N. J. Wagner and R. Castañeda-Priego, *Phys. Rev. E: Stat., Nonlinear, Soft Matter Phys.*, 2013, **88**, 060302(R).
66 N. A. Seaton and E. D. Glandt, *J. Chem. Phys.*, 1987, **86**, 4668.
67 L. V. Woodcock, *AIChE J.*, 2012, **58**, 1610.
68 K. Kremer, M. O. Robbins and G. S. Grest, *Phys. Rev. Lett.*, 1986, **57**, 2694.
69 J.-P. Hansen and L. Verlet, *Phys. Rev.*, 1969, **184**, 151–161.
70 L. L. Lee, M. C. Hara, S. J. Simon, F. S. Ramos, A. J. Winkle and J.-M. Bomont, *J. Chem. Phys.*, 2010, **132**, 074505.
71 J. C. Phillips, *J. Non-Cryst. Solids*, 1979, **34**, 153–181.
72 J. Wu, Y. Liu, W.-R. Chen, J. Cao and S.-H. Chen, *Phys. Rev. E: Stat., Nonlinear, Soft Matter Phys.*, 2004, **70**, 3–6.
73 H. He and M. Thorpe, *Phys. Rev. Lett.*, 1985, **54**, 2107–2110.